JOURNAL OF GEOPHYSICAL RESEARCH, VOL. 102, NO. B3, PAGES 5369-5384, MARCH 10, 1997

Empirical Green's function analysis: Taking the next step

S. E Hough

U.S. Geological Survey, Pasadena, California

Abstract. An extension of the empirical Green's function (EGF) method is presented that involves determination of source parameters using standard EGF deconvolution, followed by inversion for a common attenuation parameter for a set of colocated events. Recordings of three or more colocated events can thus be used to constrain a single path attenuation estimate. I apply this method to recordings from the 1995-1996 Ridgecrest, California, earthquake sequence; I analyze four clusters consisting of 13 total events with magnitudes between 2.6 and 4.9. I first obtain corner frequencies, which are used to infer Brune stress drop estimates. I obtain stress drop values of 0.3-53 MPa (with all but one between 0.3 and 11 MPa), with no resolved increase of stress drop with moment. With the corner frequencies constrained, the inferred attenuation parameters are very consistent; they imply an average shear wave quality factor of approximately 20-25 for alluvial sediments within the Indian Wells Valley. Although the resultant spectral fitting (using corner frequency and κ) is good, the residuals are consistent among the clusters analyzed. Their spectral shape is similar to the the theoretical one-dimensional response of a layered low-velocity structure in the valley (an absolute site response cannot be determined by this method, because of an ambiguity between absolute response and source spectral amplitudes). I show that even this subtle site response can significantly bias estimates of corner frequency and κ, if it is ignored in an inversion for only source and path effects. The multiple-EGF method presented in this paper is analogous to a joint inversion for source, path, and site effects; the use of colocated sets of earthquakes appears to offer significant advantages in improving resolution of all three estimates, especially if data are from a single site or sites with similar site response.

1. Introduction

Independent resolution of source, path, and site effects from waveform recordings of small-to-moderate events has proven to be an elusive goal. While several early studies relied on subjective determination of corner frequencies [e.g *Bakun et al.*, 1980; *Archuleta et al.*, 1982], many of these studies were shown to be flawed because of an incomplete accounting of the attenuation; in particular, near-surface attenuation [*Anderson*, 1986; *Hough et al.*, 1989]. Recent studies have achieved more reliable independent resolution of source and attenuation characteristics by using an empirical Green's function (EGF) method, in which attenuation effects are deconvolved from an earthquake recording by using a nearby smaller event [e.g. *Mueller*, 1985; *Frankel et al.*, 1986]; however, resolution of corner frequency can still be limited, especially for smaller events [*Hough*, 1996]. The method also requires a specialized data set: nearly colocated events with similar waveforms.

Paper number 96JB03488.

Alternatively, several studies have presented joint simultaneous inversions for source, path, and site terms [*Boatwright and Fletcher*, 1991; *Humphrey and Anderson*, 1995]. This approach is attractive because data are not limited to earthquakes for which a suitable EGF recording is available.

In spite of advances in methodology, fundamental questions remain unanswered, including the scaling relationship between stress drop and seismic moment. Because this issue is critical to various aspects of earthquake source mechanics and seismic hazard, it is important to extract as much information as possible from small-to-moderate earthquake recordings.

The scaling of stress drop with seismic moment has been debated at some length in previous studies. Because a wide range of moments is required to determine the scaling, resolution of this issue necessarily involves the determination of stress drop for small events. Most studies have focused on Brune stress drop σ_b determined from the inferred corner frequency or pulse width, assuming it to be representative of static stress drop. As discussed by *Boatwright* [1984], absolute static stress drop σ_s will depend on both the initial and final stress state of the fault, which may be impossible to

determine. The Brune stress drop, which is fundamentally an estimate of dynamic stress drop for a given rupture model, may not equal the static stress drop if the earthquake rupture deviates from the assumed model. However, if earthquake rupture processes do not depend systematically on source magnitude, the use of σ_b to investigate static stress drop scaling would be justified. That is, departures from an rupture model would contribute uncertainty to the static stress drop estimates but no systematic bias. If, on the other hand, an analysis of σ_b reveals something other than constant scaling, this would suggest a dependence of rupture processes on magnitude, which, in turn, would require a reexamination of the assumption that σ_b can be used to estimate σ_s.

While some empirical Green's function studies have suggested an increase of stress drop with moment in isolated tectonic regimes [e.g. *Guo et al.*, 1997], a compilation of results from different studies suggests no correlation [*Abercrombie and Leary*, 1993]. Although there is compelling evidence that no nonconstant scaling of stress drop can be extrapolated to events with magnitude greater than 6 [*Abercrombie and Leary*, 1993; *Hough and Dreger*, 1995; *Hough*, 1996] argues that resolution of source scaling for $M < 4$ events is limited even with empirical Green's function analysis. The pervasive lack of high signal-to-noise ratio at frequencies above 60 Hz precludes resolution of high stress drop (greater than 10 MPa) small events; bandwidth limitations of recording systems provide a further limitation. Although high signal-to-noise ratios can be recorded at higher frequencies from borehole seismometers, many such instruments have a limited low-frequency response. Borehole recordings are also considerably less abundant than surface recordings.

In light of the limitations discussed above, it is important to extract as much information as possible from the available data and to identify the resolution limits of the results. In this paper, I present an extension of the empirical Green's function analysis in which source parameters are first obtained using standard EGF deconvolution on sets of nearly colocated events. Once the corner frequencies are determined, sets of three or four spectra from colocated events are inverted jointly to determine attenuation. Residual spectra are then determined.

The method shares the same fundamental limitation of the standard EGF approach requiring a specialized data set; however, within dense aftershock sequences, clusters of multiple colocated (or nearly colocated) events are not uncommon. In this study, I use broadband recordings of M2.5-4.9 events within the 1995 Ridgecrest, California, sequence for illustration, as well as one cluster from the 1992 Joshua Tree, California, aftershock sequence for comparison.

2. Method

I first assume that the far-field seismic displacement source spectrum $\Omega(f)$ can be modeled by a one-corner model:

$$\Omega(f) = \frac{\alpha_o}{1 + (f/f_c)^c} \quad (1)$$

where α_o is the low-frequency spectral level, f_c is the corner frequency [e.g. *Brune*, 1970], and c is the asymptotic high-frequency spectral decay. c is bounded between 1.5 (required for conservation of energy) and 3; because the seismic moment scales as $1/f^3$, the omega-cube model predicts that above some frequency, large events will radiate the same high-frequency energy as small events, a prediction that is generally contradicted by observation [*Walter et al.*, 1988]. The spectral falloff has been the subject of considerable debate, with different theoretical models predicting a range of values between 2 and 3. *Haskell* [1966] proposed a model which yields $c = 3$, although this model was shown by *Madariaga* [1978] to produce infinite stress drop, while a circular crack model with a finite rupture velocity yields $c = 2$ [e.g. *Madariaga*, 1976]. *Frankel* [1991a] showed that an omega-square spectrum will result from a self-similar distribution of subevents and a constant subevent stress drop. Most observational evidence appears to favor the ω-square (c=2) model [e.g. *Hanks*, 1979; *Andrews*, 1986; *Hough and Seeber*, 1991]. In this study, both the ω-square and ω-cube models are tested.

The presence of apparent attenuation and/or site amplifications will alter equation (1) to give an observed spectrum $A(f,r)$ that can be generally written:

$$A(f,r) = A_o(f)S(f)G(r)e^{-\pi f \int \frac{dr}{Q\beta(r)}} \quad (2)$$

where $S(f)$ is the frequency-dependent site term, $G(r)$ is geometrical spreading, $A_o(f)$ is the source acceleration spectrum ($f^2\Omega(f)$), $\beta(r)$ is the shear wave velocity along the ray path, and Q is a quality factor that may include both intrinsic and scattering losses. In general, Q is also expected to vary along the raypath [e.g. *Anderson and Hough*, 1984]. As discussed by *Anderson and Hough* [1984], if observed acceleration spectra are characterized by exponential decay (i.e., a linear decay on log-linear axes), then the path integral of $(Q\beta(r))^{-1}$ can be equated with the observed spectral decay parameter κ, defined to be $1/\pi$ times the slope of the acceleration spectrum above the corner frequency when plotted on a log-linear scale. In this case, the spectral shape will be insensitive to any contribution to attenuation from a component of Q that is strictly proportional to frequency, Q_f. That is, if $1/Q_t = 1/Q_i + 1/Q_f$, where Q_t is total Q and Q_i is the frequency-independent component, then Q_f will remain unresolved. As discussed by *Frankel* [1991b], there tends to be strong trade-off be-

tween a frequency-dependent Q and geometrical spreading, and so neither tends to be resolved. In this study, I will henceforth assume a frequency-independent Q. Because Q is then determined only from spectral shape, absolute amplitudes are not considered.

Equation (2) assumes correction for an instrument response term or that instrument response is flat within the frequency band of interest. For a set of colocated events and spectra at discrete frequency points, one obtains

$$A_j(f_i, r) = A_{oj}(f_i)S(f_i)G(r)e^{-\pi\kappa f_i} \quad (3)$$

for the ith frequency and the jth event; the distance, r, site and path terms are constant.

To determine corner frequency, spectra from pairs of nearly colocated events are deconvolved:

$$R_{jk}(f_i, r) = \frac{\Omega_j(f_i)}{\Omega_k(f_i)} \quad (4)$$

That is, the common path and site effects cancel to isolate the relative source terms. If the corner frequencies are distinct from one another, estimates of equation (4) can be fit by a ratio of ω-square or ω-cube source spectra to obtain best fitting corner frequency estimates for both events (or deconvolved in the time domain to obtain a relative source time function for the larger event).

Once a set of f_c values is constrained, one can return to equation (3) and multiply the observed spectra by the shape of the source spectrum to obtain a spectrum, $P_j(f_i)$ corrected for source spectral shape:

$$P_j(f_i) = A_j(f_i, r)(1 + (f/f_{cj})^c) = C_{oj}S(f_i)e^{-\pi\kappa f_i} \quad (5)$$

where f_{cj} is the corner frequency of the jth event. C_{oj} is now a constant amplitude term that will be affected by the source amplitude, geometrical spreading, and any Q_f that is proportional to frequency. For the Ridgecrest data, it will be shown that spectra corrected in this manner do not exhibit strong apparent site effects; I therefore proceed initially to neglect $S(f_i)$ and invert each cluster of events for a common, unknown κ value. Taking the logarithm of equation (5) for a suite of events leads to a matrix equation that can be inverted linearly for A_{oj} and κ:

$$P_j(f_i) = A\vec{b} \quad (6)$$

$\vec{b}$ is given by

$$(\ -\pi\kappa \quad log(C_{o1}) \quad log(C_{o2}) \ldots log(C_{on}) \ ) \quad (7)$$

where n denotes the number of spectra. If m is the number of frequency points, A is a matrix with (mn) rows and $(n+1)$ columns:

$$\begin{vmatrix} f_1 & 1 & 0 & \cdots & 0 \\ \vdots & \vdots & \vdots & \ddots & \vdots \\ f_m & 1 & 0 & \cdots & 0 \\ f_1 & 0 & 1 & \cdots & 0 \\ \vdots & \vdots & \vdots & \ddots & \vdots \\ f_m & 0 & 1 & \cdots & 0 \\ \vdots & \vdots & \vdots & \ddots & \vdots \\ f_1 & 0 & 0 & \cdots & 1 \\ \vdots & \vdots & \vdots & \ddots & \vdots \\ f_m & 0 & 0 & \cdots & 1 \end{vmatrix}$$

The inversion of equation (6) thus yields n source amplitudes and one κ value.

As a final step, residuals between the observed raw spectra and the models are estimated. This procedure results in one unavoidable ambiguity: any common site amplification (among all events) cannot be resolved.

The method described above is henceforth referred to as the multiple-empirical Green's function (MEGF) method. As an alternative, I also consider an approach that bypasses the initial EGF deconvolution and thus avoids the numerical instabilities associated with deconvolution. In the absence of significant site effects, the above procedure can be revised to consider a hybrid inverse (for brevity, henceforth referred to as HI) method in which a suite of spectra from a cluster are fit jointly for corner frequencies and κ. This problem is nonlinear in f_{cj}; however it is possible to consider a HI/parameter search approach, in which the observed spectra are multiplied by a source spectral shapes with a range of corner frequencies (that is, a range for each event) to obtain the suite of f_{cj} values and single κ value that is optimal. This involves a procedure similar to that outlined above, except that the observed spectra are multiplied by a suite of source spectral shapes rather than one that is previously constrained:

$$P_j(f_i) = (1 + (f_i/f_{cj,t})^c)A_j(f_i, r) \quad (8)$$

where $f_{cj,t}$ is the trial corner frequency for the jth event. If we allow a trial of C corner frequencies for each event, then this inversion is performed Cn times. However, the parameter search can be done first over a coarse grid of corner frequencies and then repeated with a more narrow range of trial event-specific corner frequencies. The optimal set of corner frequencies (and κ) is chosen to be the one that optimizes the collective least squares residual.

3. Case Study: The Ridgecrest Sequence

The 1995 Ridgecrest sequence began with a M5.4 event on August 17, 1995 [*Hauksson et al.*, 1995] (Figure 1a). This sequence, which also produced a $M5.8$ event

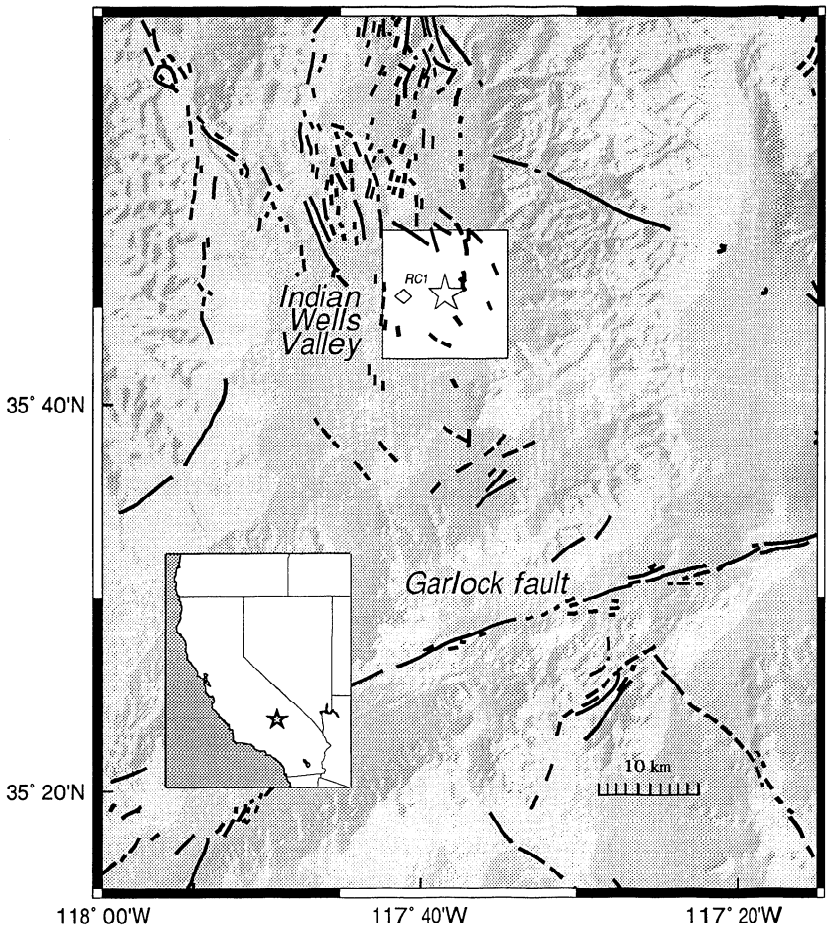

Figure 1a. Setting of Ridgecrest earthquake sequence, including regional faults and topography (grey scale). The September 20, 1995, $M5.8$ mainshock is indicated by a large star; small diamond indicates station RC1. Open square is centered at same location as map shown in Figure 1b but not drawn to scale. The Indian Wells Valley is flanked by the southern tip of the Sierra Nevada to the west and the Argus Range to the east. Inset at lower left indicates position of Ridgecrest (star) within California.

on September 20, 1995, and a $M5.2$ event on January 7, 1996, represents the largest seismic events to be observed in the immediate region since the inception of the Southern California Seismic Network (SCSN) catalog. The sequence occurred within the Indian Wells Valley, south of the Owens Valley and flanked by the Sierra range to the west and the Argus range to the east (Figure 1). Borehole logs reveal a depth-to-basement of approximately 1.6 km in the epicentral region, with the upper layers composed primarily of alluvium with some interbedded basalt. Events in the 1995–1996 sequence are aligned with a broad N-NW trending system of small faults. Focal mechanisms reveal a mixture of mostly right-lateral/normal/oblique events consistent with the expected regional right-lateral shear and extension of the Owens/Indian Wells Valley region. Following the August 17, 1995, event, three portable digital seismometers were deployed in the epicentral region. The sites were instrumented with United States Geological Survey (USGS) developed GEOS recorders [*Borcherdt et al.*, 1985] and a dual gain sensor configuration including a Mark-Products L-22 2-Hz weak-motion sensor and a Kinemetrics force-balance accelerometer (FBA). The sample rate was 100 samples per second on all six channels. One of these sites was still in place at the time of the $M5.8$ September 20, 1995, event, although that event was not recorded due to an unrelated previous power failure at the site. In this study, I analyze data from the one longer-term site, RC1, because of the significantly higher number of recordings available from this station. Because both the $M5.4$ and the later $M5.8$ events had extensive aftershock sequences, RC1 recorded an abundance of events of $M3$ and greater; the largest recorded event was a September 24, 1995, $M4.9$ aftershock of the September 20, 1995 mainshock. The recorded events are associated with events in the SCSN catalog; the network locations and magnitudes will be used in this study.

In this study, I use recordings of events with high signal-to-noise ratios on the FBA channels to avoid uncertainties associated with the L-22 instrument response at frequencies near and just below its natural

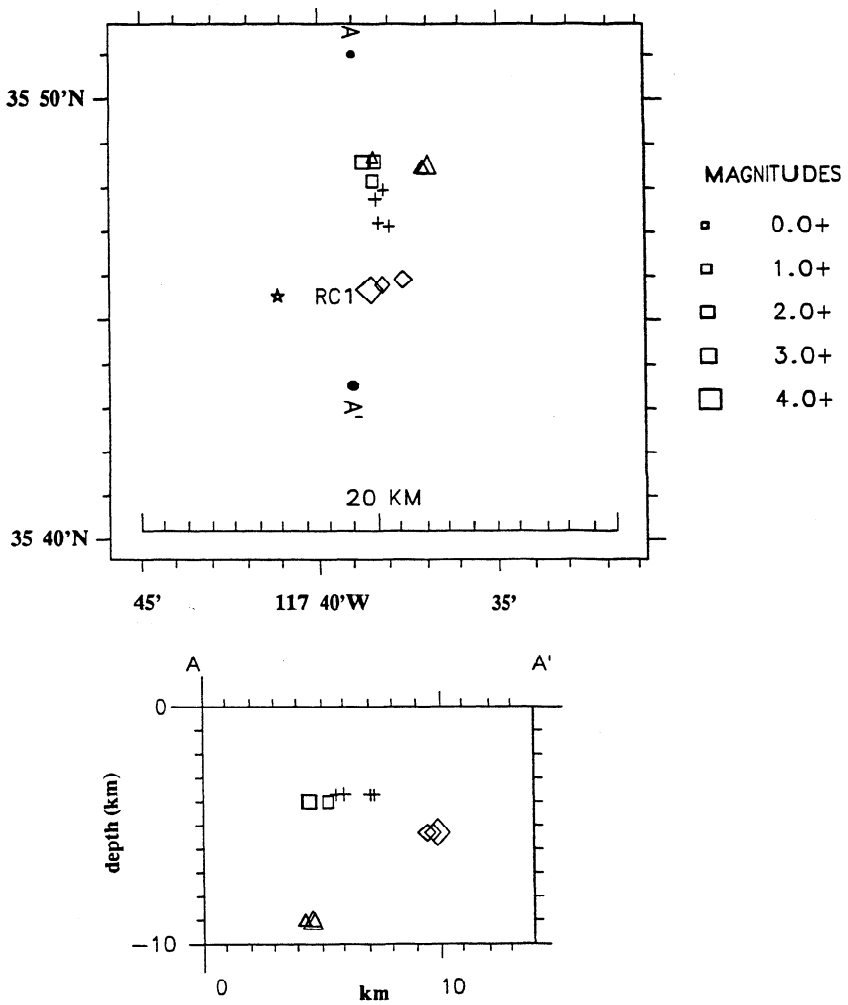

Figure 1b. Portable station, RC1, that provided data used in this study (small star). Locations of events analyzed are shown by other symbols, with size scaled to magnitude as shown at right. For clarity, depths within each cluster are fixed to a representative event depth for each cluster; actual values are listed in Table 1. Clusters 1, 2, 3, and 4 are represented by crosses, triangles, diamonds, and squares, respectively. One event is used for both clusters 2 and 4; it is shown here as a triangle.

frequency. Because of the short epicentral distance, events with magnitudes as small as $M \approx 2.4$ can be used.

Figure 2 shows one component of motion for four event clusters that were judged to provide suitable event suites for analysis. Parameters for the events are listed in Table 1. To refer to a given event, I will henceforth use Julian day, hour, and minute (e.g., 2680427=day 268, 0427 GMT). Figure 1b shows event locations, with depths fixed to be representative of the average for each cluster; Table 1 lists actual depths for each event. In most cases, events within a cluster are separated by less than a few kilometers in hypocentral distance. One exception is cluster 2, which includes one event (2680427) that is 4-5 km shallower than the other two events in the cluster. In spite of this depth difference, Figure 2 reveals a good level of waveform similarity with the other two events, and so it is included. I note that although the largest event in cluster 2 (2680447) is the largest of the recorded data set (M4.9), no early aftershocks of this event were recorded because the trigger itself filled the available space on the GEOS data tape (in general, the very earliest aftershocks often provide the best empirical Green's function events).

The four suites span magnitude ranges of 2.6-3.9, 2.6-3.8, 2.4-4.9, and 2.5-3.8 (a fifth possible cluster was not used because of conspicuous near-field phases in the waveforms). To calculate spectra, I use 4-s to 5-s windows (consistent over a given cluster) bracketing the direct S arrivals using a cosine taper over 10% of the series length at both ends. A standard fast Fourier transform (FFT) is used to calculate spectra using a boxcar smoothing window of 0.3 Hz. I calculate root-mean-square averages of the two horizontal components for all analysis and focus on a frequency range of 1-20 Hz.

The first cluster of events consists of four events, three with magnitudes of 2.6, 2.7, and 3.8 that occurred

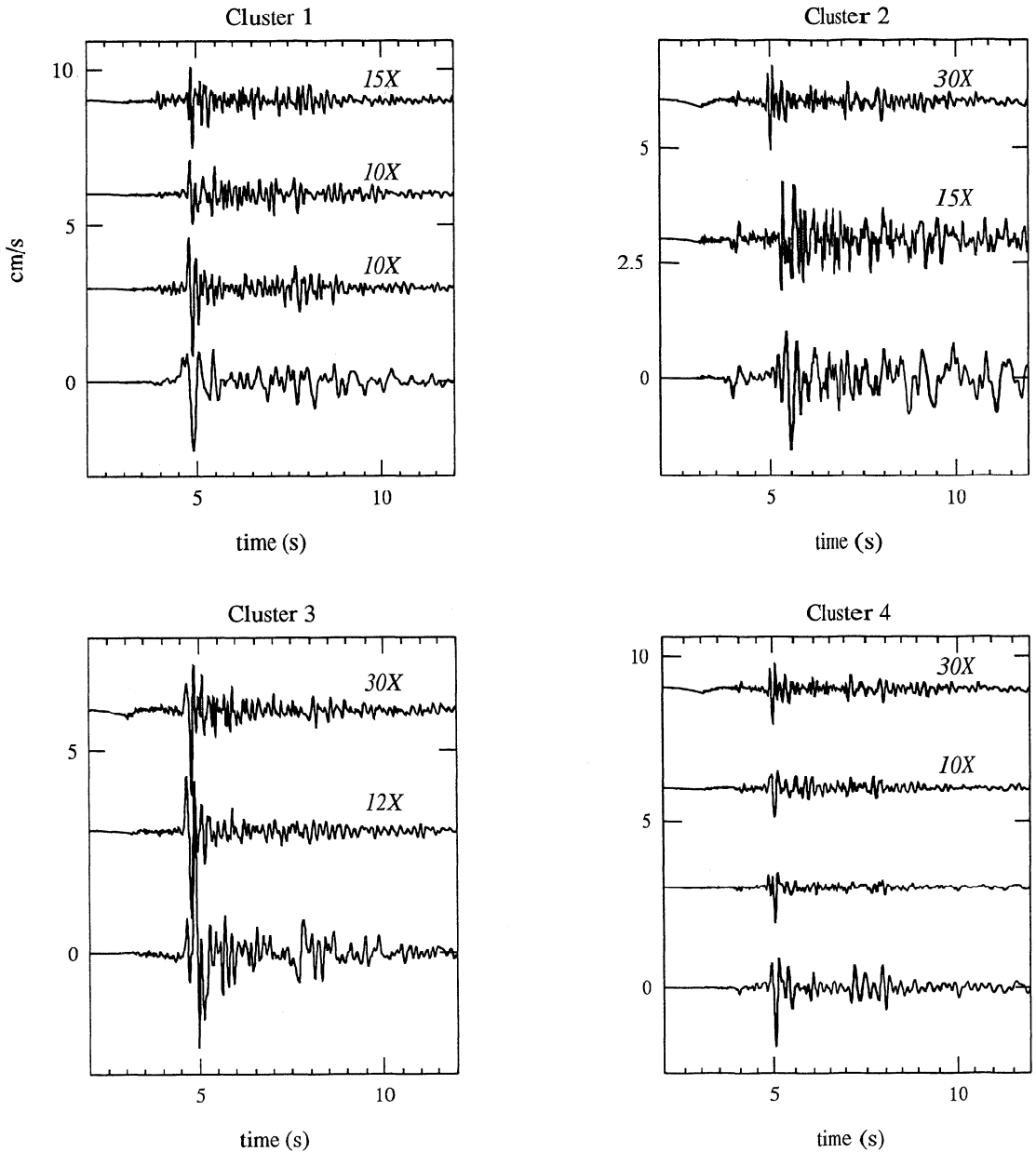

Figure 2. Scaled, offset north-south components of seismograms for earthquakes in each cluster used in this study. Acceleration (FBA) channels are integrated to obtain velocity and high-pass filtered above 0.3 Hz. Time series are scaled by peak ground motion by factors shown (or unscaled if no factor is given) and offset to illustrate waveform similarity.

within a 7-min span on Julian day 242 and another magnitude 2.6 event that occurred on day 243. Figure 3 shows deconvolutions for source spectra using each of the three smaller events as the EGF; in each case, inversion results using both ω-square and ω-cube models are shown. The least squares misfit is approximately 20 – 70% lower using the ω-cube model. Figure 3 reveals that this model is better able to fit the relatively sharp inferred corner frequency of the larger event. In one case, the ω-square model is unable to match the shape of the deconvolved source spectrum. As can be seen in Figure 4, this suite of events is consistent with an ω-cube model, because the high-frequency levels are nearly indistinguishable for all events.

The other three clusters are analyzed similarly using standard EGF analysis (Figure 3); in each case, no compelling results are found to support the ω-cubed model. I thus assume the ω-square model for these clusters. One pair of events (2711136 and 2720015, cluster 4) yielded a deconvolved source spectrum estimate that was observed to be noisy, with prominent high-frequency peaks resulting from holes in the empirical Green's function spectrum. Based on a similarity in low frequency ($f < 10$ Hz) spectral shape of this ratio to the ratio between events 2750010 and 2720015, I assign to event 2711136 the same f_c value, 3.5, obtained for event 2750010.

Once the corner frequencies are constrained, the un-

Table 1. Event Clusters

Cluster	Day	Time, GMT	Latitude	Longitude	Depth, km	log(M_o)	f_{cs}	σ_s	κ
1	242	1554	35.7957	-117.6400	3.72	15.95	2.2	3.7	0.075
	242	1551	35.7867	-117.6387	3.36	14.00	9.6	3.4	
	242	1558	35.7853	-117.6330	3.62	14.15	5.8	1.1	
	243	0255	35.7990	-117.6358	4.83	14.00	14.0	10.6	
2	268	0421	35.8080	-117.6185	8.75	15.34	5.0	53.3	0.057
	268	0427	35.8115	-117.6413	4.72	13.70	16.0	10.6	
	268	0447	35.8087	-117.6162	9.40	17.45	1.7	7.9	
3	264	2348	35.7613	-117.6425	5.44	16.11	2.0	4.0	0.052
	264	2353	35.7631	-117.6365	5.26	14.15	3.9	0.3	
	265	0006	35.7653	-117.6263	5.44	16.11	2.0	4.0	
4	271	1136	35.8098	-117.6402	4.40	15.34	3.5	3.7	0.062
	272	0015	35.8023	-117.6413	3.80	14.00	8.0	2.0	
	275	0010	35.8095	-117.6455	4.72	15.80	3.5	10.5	
	268	0427	35.8115	-117.6413	4.72	13.70	19.0	13.3	

Assigned cluster number; Julian day (1995), and hour and minute of event. Moments are determined by scaling relationship proposed by [*Hanks and Boore*(1984)] using SCSN magnitudes; value listed is log(M_o), with M_o in Newton-meters. f_{cs} and σ_s are corner frequencies and stress drops (in megapascals) determined from S waves (parentheses indicate assigned value); κ is inferred spectral decay parameter for each cluster

corrected velocity spectra are used in an inversion to find amplitude terms A_oj for each spectrum and a common decay parameter, κ. This procedure yields the spectral fits shown in Figure 4, which are observed to be (subjectively) quite good in all cases. Optimal κ values of 0.075, 0.057, 0.052, and 0.062 are found for clusters 1, 2, 3, and 4, respectively; the implications of these values for Q structure are discussed below.

As a final step, residuals are calculated between all spectra and models shown in Figure 4. This is done for each individual spectrum and the results are then averaged within each cluster. Figure 5 shows the final inferred residuals, which are observed to be very consistent among the clusters.

I now apply the HI procedure described in the section above. Figure 6 shows spectra and model fits for cluster 3, indicating the resulting corner frequency estimates from both methods. It is observed that using the HI method, corner frequency estimates are generally higher for the large events and lower for the smaller ones. This effect is seen consistently among the other clusters; these results are not shown.

4. Results From the Joshua Tree Sequence

For the purpose of comparison, I repeat the above analysis on one cluster of aftershocks from the 1992 M6.1 Joshua Tree, California, earthquake [*Hauksson et al.*, 1993]. The full set of portable GEOS aftershock data for this event have been analyzed previously using a standard eGf approach to obtain corner frequencies [*Hough and Dreger*, 1995, herein after referred to as HD95]. Here I use recordings from station FVS, on the northern edge of the Coachella Valley to the south of the Joshua Tree epicenter (see HD95 for details). Two of the three events analyzed correspond to events 22 and 80 of HD95: a M2.3 event on Julian day 118 (1992) and a M5.0 event on day 139. A third event analyzed occurred approximately 47 seconds after the M5.0 event; it is not listed in the SCSN catalog and was not analyzed by HD95. Its inclusion was initially based on an observation from the Ridgecrest sequence, that temporally clustered events seem to correspond to spatially clustered events (i.e., good EGF events). Based on a comparison of long-period displacement spectral levels, I estimate a M3.6 for this event.

Figure 7 presents one component of the waveforms for this cluster of events. Figures 8 and 9 show the deconvolved source spectra, velocity spectra (with best fitting models), and residuals, analogous to Figures 4, 5, and 6.

As a further illustration, I analyze this cluster using the second, HI, method. Corner frequency estimates from the two methods are shown in Figure 9. In this case, the biases associated with the HI method are even more pronounced: while the MEGf method resolves distinct corner frequencies of 2 Hz, 6.3 Hz, and 11 Hz corresponding to the magnitude 5.0, 3.6, and 2.3 events, respectively, the HI method yields corner frequencies near 6.5 Hz for all three events. This bias results from apparent resonance peaks in the residual spectrum near 3.5 and 10 Hz; I will discuss these results in the following section.

5. Interpretation: Source, Path, and Site Effects

5.1. Stress Drop

To interpret the inferred corner frequency values for source parameters, I use the standard formulation [*Keilis-Borok*, 1959]

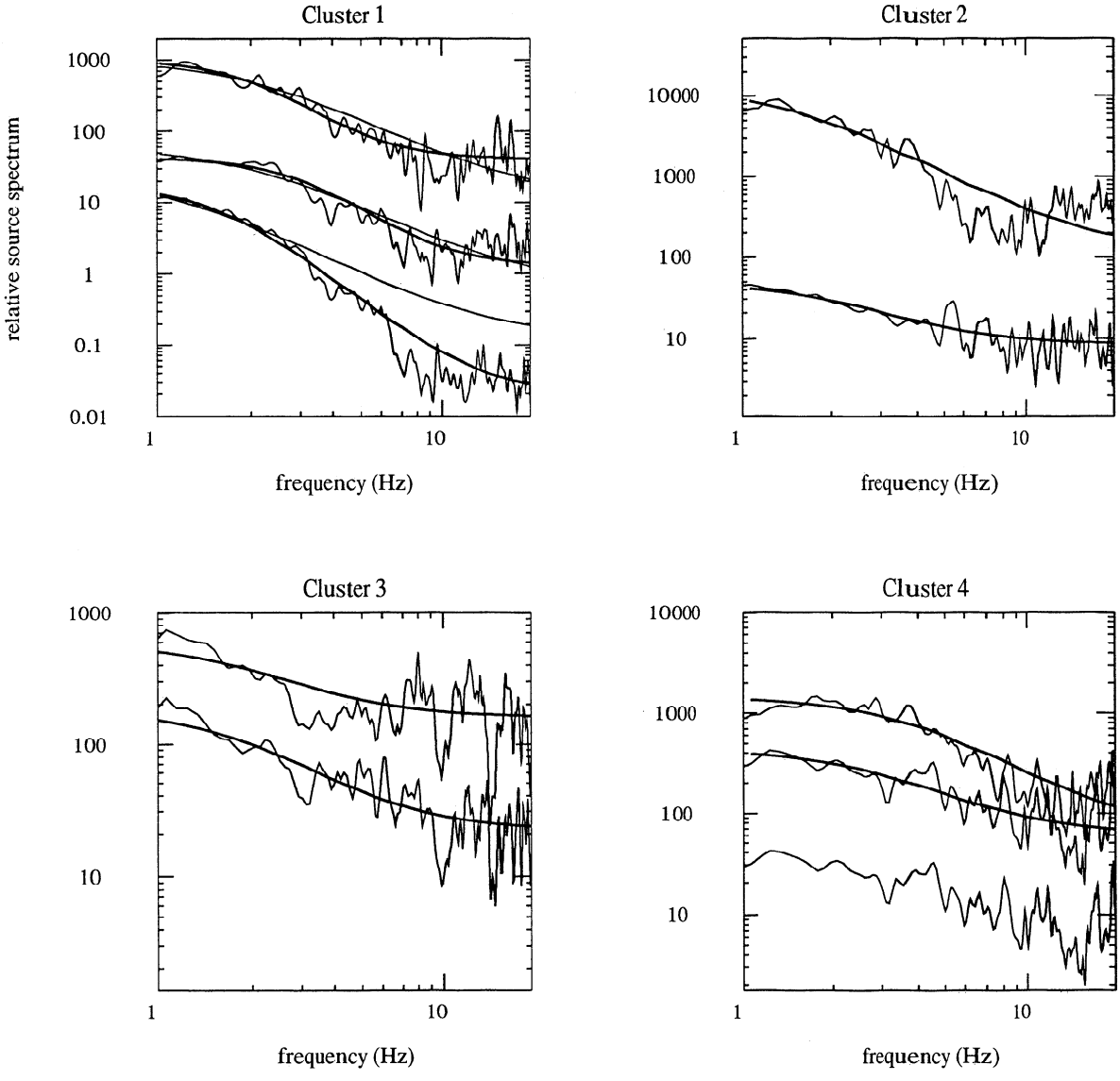

Figure 3. Deconvolved relative source (rms-averaged) spectra from clusters 1-4 using smaller events as empirical Green's functions. For cluster 1, the light solid line shows the best fitting ratio of ω-square source models; dark solid line shows best fitting ratio of ω-cube models. The latter is observed to provide a significantly better fit to the sharp corners evident in the deconvolved source spectral ratio. For clusters 2-4, only the best fitting ω-square ratio is shown. No fit is shown for one of the events in cluster 4 because high-frequency noise levels preclude a stable regression; however, the spectral shape below 10 Hz is observed to be extremely similar to the other two deconvolved source spectra in this cluster.

$$\sigma = M_o\left(\frac{f_c}{0.49\beta_s}\right)^3 \quad (9)$$

where β_s is the shear-wave velocity at the source. The seismic moment M_o, is estimated using the moment-magnitude relationship developed by *Hanks and Boore* [1984], $log(M_o) = 1.5M + 16.1$, where I assume that the local network magnitude provides an estimate of the moment-magnitude. Although uncertainty in absolute stress drop level is introduced by several factors, including the choice of β_s in equation (9), in general, it is expected that relative stress drop estimates will be better resolved. I use a P wave velocity model from J. Mori (personal communication, 1996) (Table 2) and assume a V_p/V_s ratio of 1.7, giving a β_s of 2.8 km/s. Stress drop values for the nine events are listed in Table 1 and shown in Figure 10; they are found to be consistent, generally of the order of 1-10 MPa.

The one stress drop value appreciably over 10 MPa corresponds to the largest event in the data set, magnitude 4.9. It is possible that the low-frequency bandwidth cutoff, caused mainly by low signal/noise ratios of the smaller events, results in a bias for this event. Although an increase of stress drop with moment is suggested, Figure 11 also indicates the limits in reso-

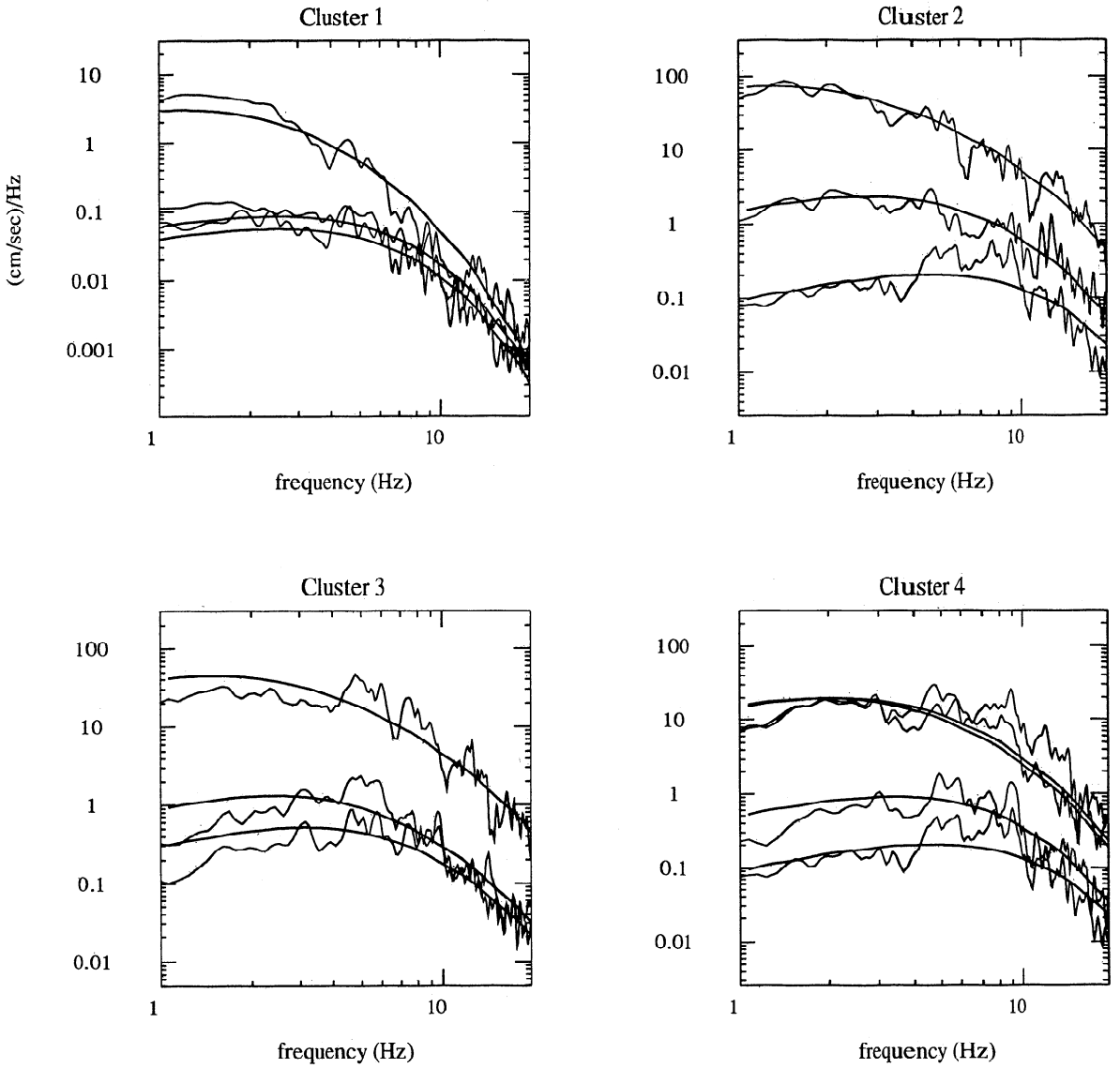

Figure 4. Estimated (uncorrected) relative velocity spectra for all clusters are shown (rms average of two horizontal components); solid line gives best fitting model with corner frequency constrained from empirical Green's function analysis and common κ value fit by simultaneous inversion of all spectra in each cluster.

lution associated with a frequency bandwidth of 1-20 Hz. These limits may be slightly generous in that is assumes resolution of corner frequencies all the way up to the bandwidth bounds. Similarly, Figure 10 reveals an inability to resolve stress drop values appreciably above 10 MPa for the smallest events in the data set.

I also note that the cluster with the highest overall stress drop values (cluster 2) is also the deepest. As suggested in previous studies [e.g. *Jones and Helmberger*, 1996], this could indicate a tendency of stress drop to increase with depth. However, it could also, at least in part, reflect an inappropriate choice of β_s in equation (9). In general, a constant value used for a suite of events may result in a bias of stress drop values (towards high values) for deep events. If stress drop estimates for cluster 2 are recalculated using β_s of 3.2 km/s (more appropriate for 9 km depth), all values are reduced by a factor of 1.5. The M4.9 event remains as the highest stress drop event, but with a value of 36 MPa, somewhat more in line with other events (the value for the M3.5 event in this cluster is reduced to 7.1 MPa).

The corner frequencies for the Joshua Tree events imply somewhat higher stress drop values in general: 2, 30, and 124 MPa for the magnitude 5.0, 3.6, and 2.3 events, respectively, using β_s of 2.8 km/s. It is likely that this β_s value is inappropriately low for the Joshua Tree events; using the preferred value of 3.64 km/s from HD95 lowers the stress drop estimates to 0.9, 14, and 56 MPa, respectively. Although it is again possible that the low-frequency cutoff biases the corner frequency/stress drop estimates for the M5.0 event, these results are consistent with somewhat higher stress drop

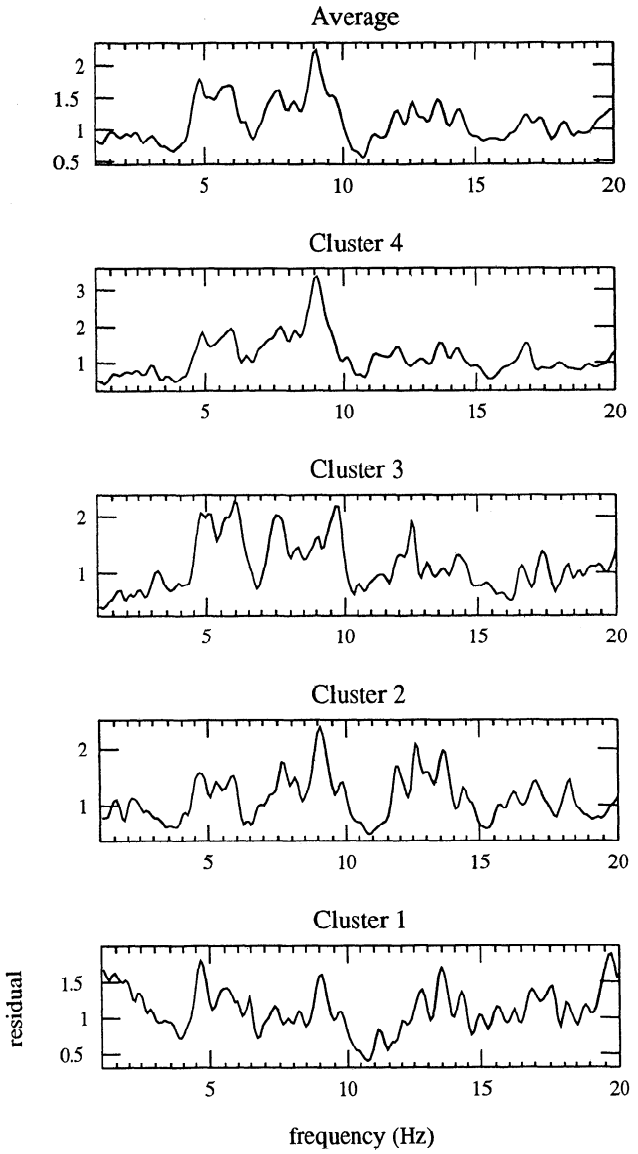

Figure 5a. Residuals between spectra and models for each cluster are shown in the bottom four panels. For each cluster, residuals between spectra and models are averaged over all events. The top panel shows final residual averaged over all clusters.

results for the Joshua Tree events than for Ridgecrest events.

5.2. Attenuation

The inferred κ values from the Ridgecrest events can be interpreted using the plane layer velocity model, as illustrated schematically in figure 11. Assuming constant Q and a representative hypocentral distance of 8 km, a κ of 0.06 implies a shear wave Q value of approximately 70. More plausibly, attenuation is expected to increase significantly with depth [e.g. *Hough and Anderson*, 1988]. The earthquakes occurred within the Indian Wells Valley, in a region where depth to basement is estimated at approximately 1.6 km (a number of boreholes, flanking the epicentral region, have penetrated to basement (A. Katzenstein, personal communication, 1996). Assuming a standard, shallow bedrock Q value for 1.6-5.0 km depth, the dominant contribution to κ will come from the portion of the ray path through the valley itself. Differentiating between a basement Q, Q_b, and a Q within the 1.6-km-thick alluvial sediments, Q_a, this dominance can be illustrated with a consideration of reasonable values for Q_b. For example, a Q_b of 500 yields a Q_a of 18-20 (for a κ of 0.06). Because any plausible Q_b value for the basement rock is much higher than these values, the Q_a results are fairly insensitive to the choice of Q_b. For example, lowering Q_b to 200 only raises Q_a values to 20-25. These results are consistent with other field and in situ attenuation measurements of shallow alluvial sediments [e.g. *Joyner et al.*, 1976]. A Q_a value on the order of 20-25 is somewhat low for the entire 1.6-km-thick valley. However, it is likely that the inferred κ value represents a path average of lower Q_a values in the very uppermost layers and somewhat higher values at depth. Because $1/Q_a$ is the physically meaningful quantity, even relatively thin layers of very low Q material will provide dominant overall contributions.

The four κ estimates are actually consistent with the small differences in ray paths for each cluster caused by an epicentral distance range of 4-8.5 km and a source depth range of roughly 4-9 km. As revealed in the inset to Figure 11, κ correlates not with the overall hypocentral distance but with the length of the ray path through the valley itself. If I consider each ray path and κ value separately, assuming a Q_b of 500 and estimating the ray path length through the valley, I obtain separate Q_a values that vary between 18.5 and 20.3.

5.3. Site Response

The spectral residuals presented in Figure 5 are expected to incorporate a number of unmodeled effects, including possible differences in source depth and/or focal mechanism between an earthquake and its EGf event. However, the character of the residuals shown in Figure 5 are quite consistent with the expected shape of one-dimensional resonance modes caused by near-surface sedimentary layers. A P wave velocity model for the Ridgecrest region was developed independently (J. Mori, personal communication, 1996) for earthquake location. As a starting model, I modify the depth of the top layer to reflect the local depth to basement and use a standard Poisson's ratio to obtain the S wave velocity model shown in Table 2. This model incorporates Q values that are deliberately chosen to be too high, because the MEGf method resolves shallow attenuation as a path, rather than a site, effect.

I use the reflector matrix technique of *Kennett and Kerry* [1979] to compute the theoretical one-dimensional response of the velocity model to vertically incident S waves. The full extent of the Indian Wells Valley causes a fundamental resonance peak at a frequency lower than that observed. To match the inferred residuals, I add a

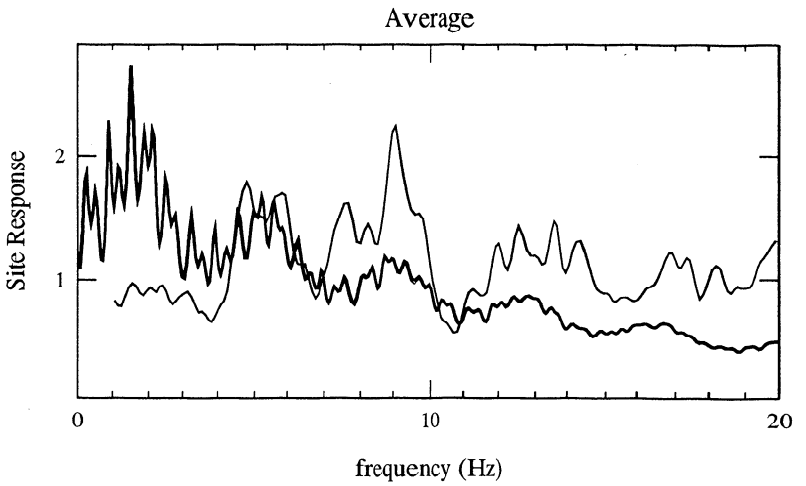

Figure 5b. The solid line indicates the theoretical one-dimensional response of the S-wave velocity model shown in Table 2 (J. Mori, personal communication, 1996), with depth-to-basement estimated based on borehole information (A. Katzenstein, personal communication, 1996) and a shallow lower-velocity layer added to match observed residual shape.

shallow layer (170 m) with a lower velocity (1200 m/s). These values are poorly constrained because the resonance modes are controlled only by the ratio of velocity to layer thickness. In Figure 5b, I compare the final model to a final spectral residual that is averaged over the four clusters. A further source of uncertainty (in using observed residuals to infer velocity structure) results from the neglect of angle of incidence in the theoretical response calculation. However, as illustrated by Figure 11, while there is a considerable range in inci-

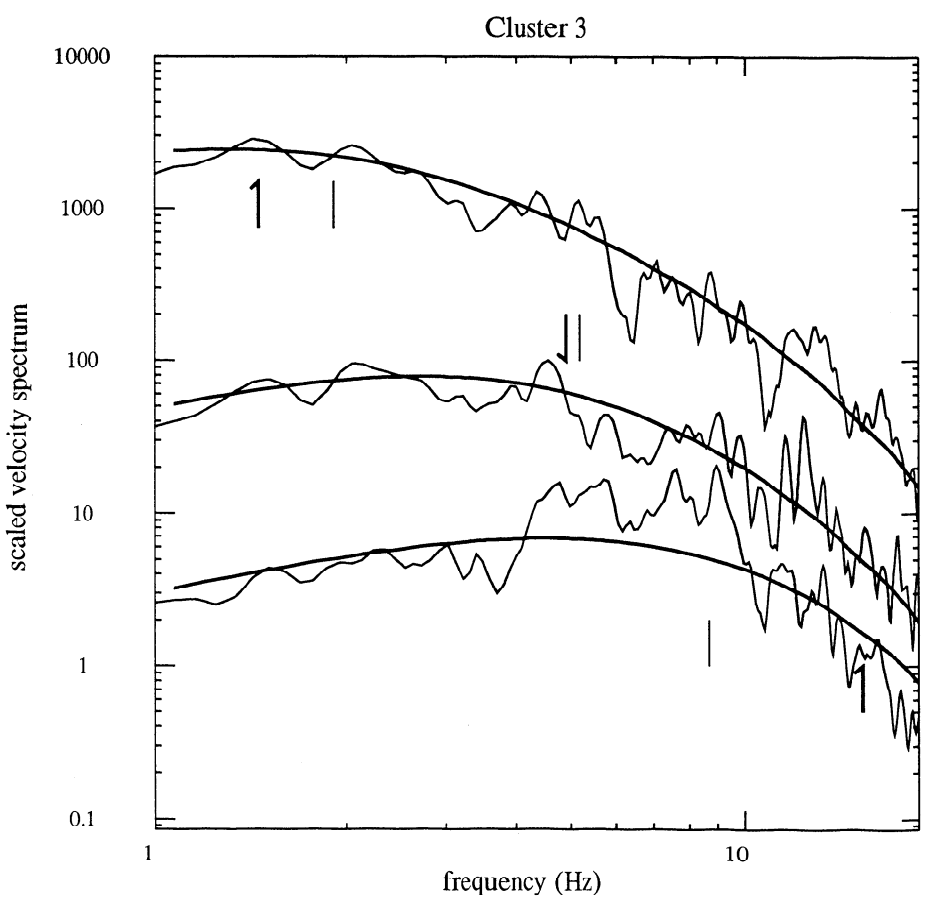

Figure 6. Velocity spectra (rms average of horizontals) from cluster 3 are shown along with corner frequency estimates (light tick marks) resulting from simultaneous inversion for source and attenuation terms; dark arrows indicate preferred corner frequency estimates from EGF analysis.

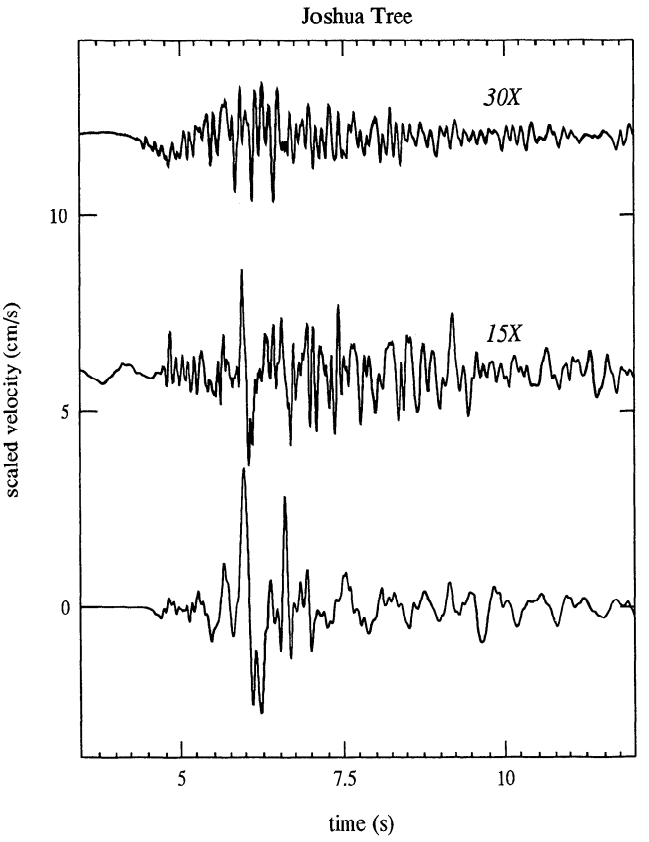

Figure 7. N-S component of velocity for three events comprising a cluster from the 1992 Joshua Tree aftershock sequence. Events are scaled by factor shown and offset for clarity.

dence angle within the data set, Figure 5a reveals the individual cluster residuals to be consistent. The choice to average all results stems from this observed consistency. The comparison between absolute amplification levels is reasonably good (Figure 5b); the low inferred amplitude of the fundamental mode may reflect relatively low signal-to-noise levels of the empirical Green's function events analyzed at the longer periods. . Given that κ is determined before site response in this inversion procedure, it is also possible that a strong fundamental mode could systematically bias all κ estimates (towards higher values), thus effectively mapping site response into the path term. However, plotting the acceleration spectra obtained here on log-linear axes [e.g. *Anderson and Hough*, 1984] revealed that the spectra are well-characterized by an exponential decay shape, with no conspicuous peaks near 1-3 Hz that would bias κ estimates.

The average final residual for the Joshua Tree cluster (Figure 9) also suggests a site response resonance, with somewhat broad harmonic peaks near 1.5, 3.5, and 10 Hz. The inferred site response in this case is less well resolved than that inferred for the Indian Wells Valley because it results from analysis of only a single cluster. However, the residual is qualitatively consistent with subtle site response caused by sediments within the Coachella Valley. Presumably, this sedimentary valley will produce substantial site effects; however, station FVS was located at the northern valley edge, presumably on fairly thin sediment cover.

6. Discussion and Conclusions

I have presented an extension of the empirical Green's function method in which the constraint of corner frequencies is used to provide high-resolution estimates of attenuation for a suite of events even for a single site. This method can be applied to clusters of any size.

Applying the method to a set of M2.4-4.9 events from the 1995-1996 Ridgecrest sequence, I find the results to be stable and consistent. Corner frequency results imply Brune stress drop values almost exclusively in the range 1-10 MPa, with no resolved scaling of stress drop with moment. The stress drop estimate of the M4.9 event is high, 53 MPa, but may reflect borderline signal-to-noise at the longer periods (in particular, signal-to-noise levels of the Green's function events). In general, this method, as presented here, is best suited to analysis of small-to-moderate events, perhaps M2-4.5, because, at larger magnitudes, the point-source assumption is no longer appropriate. However, the method could be extended to allow for finite-fault inversions, along the lines of previously EGf analysis of small events from the

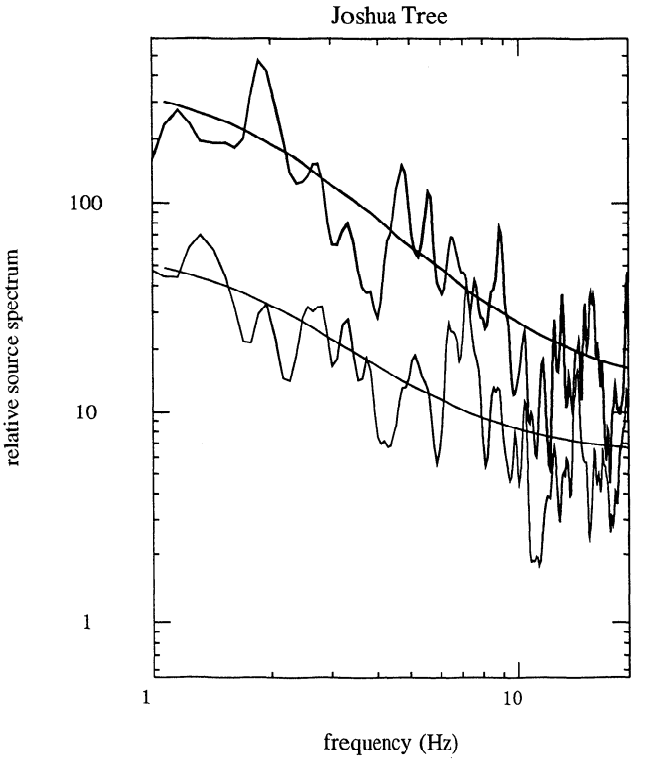

Figure 8. Deconvolved relative source spectra (rms-average of two horizontal components) for Joshua Tree events; the two spectra result from use of the M3.6 and M2.3 events as empirical Green's function. The solid line indicates the best fitting ratio of ω-square models.

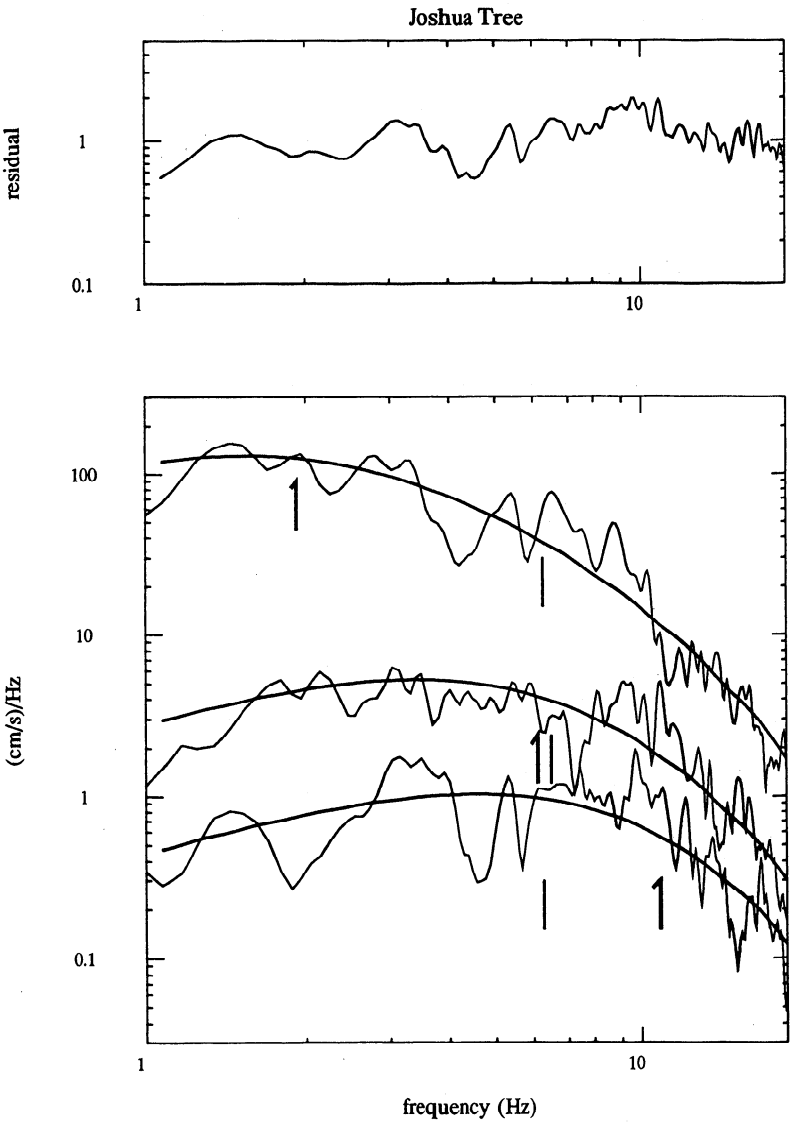

Figure 9. (bottom) Joshua Tree velocity spectra (rms average of horizontal components) for the three events; solid lines indicate best fitting models incorporating (preferred) corner frequencies from figure 8 and optimal κ value. Small dark arrows indicate corner frequency estimates from EGF analysis; light tick marks indicate corner frequency estimates from simultaneous inversion. (top) The residual spectrum, averaged over the three events.

Table 2. Model

Z, km	α, km/s	β, km/s	ρ, kg/m^3	Q
0.17	3.00	1.2	1800	20
1.40	3.55	2.0	1800	50
1.40	3.76	2.17	2400	200
9.00	4.80	2.80	2800	500
10.00	5.52	3.20	2800	500

Thickness of layer (Z), P and S wave velocities(α and β), density (ρ), and quality factor (Q). The Q value for the first layer is determined from observed spectral shapes; Q values are assumed for the deeper layers. These Q values will trade off to some extent, as discussed in the text.

San Jacinto, California region [*Frankel et al.*, 1986] or M5-6.7 regional events [*Mori and Hartzell*, 1990; *Dreger*, 1994; *Hough and Dreger*, 1995].

The attenuation and site response results from this study yield a relatively low Q_o value, 20-25, for the mostly alluvial sediments within the Indian Wells Valley. It is likely that this value represents an average over the 1.6-km extent of the valley, with lower Q_o over the upper few hundred meters and somewhat higher Q_o at depth; such a gradation cannot be resolved with surface recordings of earthquakes that all occur below the basement. The inferred Q structure corresponds to a t^* value of 0.05 (the minimum estimated value of κ from this study).

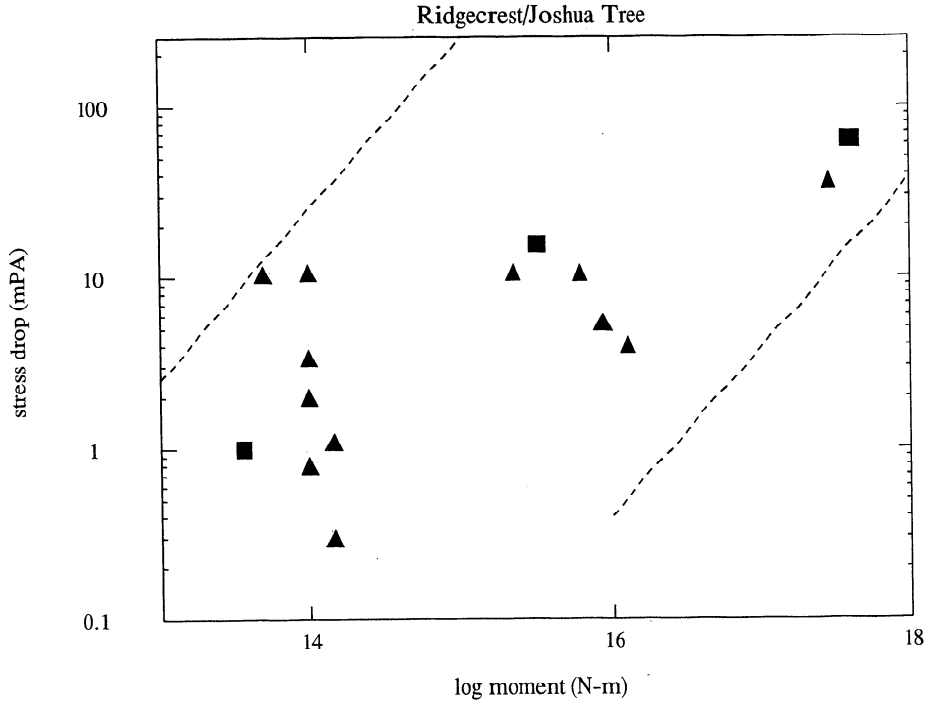

Figure 10. Preferred Brune stress drop results are shown for Ridgecrest events (triangles) and Joshua Tree events (squares). The dashed lines indicates the limits in stress drop resolution imposed by a minimum resolved corner frequency of 1 Hz and a maximum of 20 Hz; any moment-stress drop pair outside these lines would not be resolvable with the available data.

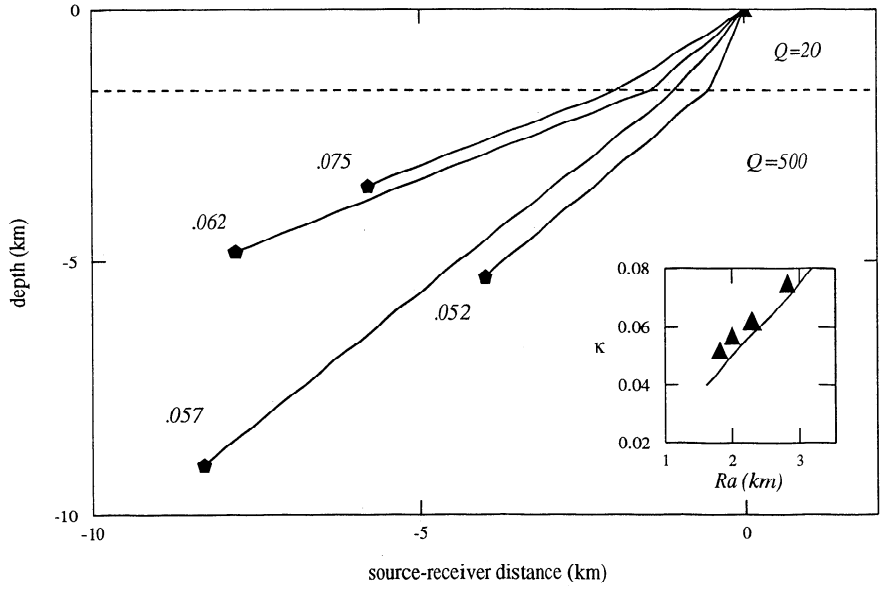

Figure 11. Cartoon illustrating raypaths for four analyzed event clusters and interpretation of inferred κ values (s) in terms of layered Q_a structure. The dashed line indicates the depth to basement of the Indian Wells Valley in the vicinity of the epicenter (in reality, the basement is not flat, but κ values are expected to reflect a local depth to basement, as illustrated). The basement Q_b value is assumed; the Q_a value is inferred from the κ results. A good correlation is noted between κ and the length of the ray path, Ra, within the Indian Wells Valley sediments; increased ray path within the higher-Q basement does not appear to contribute significantly to κ estimates. Small inset shows κ values versus estimated raypath length through the valley (in kilometer); solid line indicates a Q_a of 20. The line falls slightly below all four points because it neglects the small contribution to κ from propagation through the basement; however, the slope is well matched and the scatter is small.

Anderson [1986] shows the bias in corner frequency that will result from neglecting a range of κ values. His results show that, for κ=0.05, corner frequency will be underestimated by factors of about 8, 2, and 1.2 for moments of 10^{13}, 10^{15}, and 10^{17} Nm, respectively (i.e., M_w values of 1.9, 3.9, and 5.9). Thus, neglecting the near-surface attenuation at site RC1 would bias stress drop values by a factor of nearly 6 for M_w4 events and by a factor of 1.6 for M_w6 earthquakes. This reveals significant potential biases in source parameter estimation resulting from near-surface attenuation, even for moderate magnitudes recorded at short epicentral distance.

It is instructive to consider potential biases revealed in this study, in particular, the effect of even subtle site response resonance peaks on corner frequency estimates. Although standard EGf deconvolutions should be successful in removing any linear site response, standard joint inversions for source, path, and site effects may not be successful in distinguishing corner frequencies from resonance peaks. Applying the restricted source/path inversion to the entire Ridgecrest data set, I observed a tendency for the small-event corner frequencies to cluster near the 5-Hz resonance peak (as can be seen in the example presented in Figure 7), even though the spectra are not characterized by the dominant site response effects seen in other regions. A similar, perhaps stronger, bias is revealed in analysis of the Joshua Tree cluster.

Previous joint inversions [*Boatwright and Fletcher*, 1991; *Humphrey and Anderson*, 1995] have included an unknown site response term that is not incorporated in the HI method. Although it would be possible to include an additional site response term in the HI method as presented here, it is clear that if the data set includes recordings from a limited number of sites (or sites with similar site response), one would have very limited resolution between subtle resonance peaks and an f_{max} corner frequency effect [*Hanks*, 1979]. Ideally, a joint inversion could be made with the added constraint that the residual spectrum, assumed to be site response, be modeled as a set of harmonic peaks; however, this constraint is difficult to implement. In contrast, the stability of the κ and site response estimates obtained using the MEGf method suggests that modest site response peaks do not significantly bias estimates of path effects if corner frequencies are previously constrained. Conceptually, this result is not surprising; spectral decay estimates will be constrained by the shape of the spectrum over the full bandwidth. The MEGF method thus appears to offer significant advantages in the independent determination of source, path, and site effects, even if data are available from only a single site.

Acknowledgments. The author is most thankful to Allan Katzenstein and Frank Monastero for assistance with challenging fieldwork logistics; I thank Jim Mori for providing his velocity model and helpful discussions/information through the course of this investigation; Dave Wald for GMT tips; Art Frankel, Ned Field, Brian Cohee, an anonymous reviewer, and the Associate Editor for their helpful reviews; I thank Gary Glassmoyer and Chris Dietel for their patience and help in overcoming data-playback hurdles. Figure 1a was generated using GMT software [*Wessel and Smith*, 1991]. Finally, I thank William Hinze for unfailing professionalism, and Mary Sue Hough for making it a pleasure to travel to Ridgecrest.

References

Abercrombie, R. and P. C. Leary, Source parameters of small earthquakes recorded at 2.5 km depth, Cajon Pass, California: Implications for earthquake scaling, *Geophys. Res. Lett.*, *20*, 1511–1514, 1993.

Anderson, J. G, Implication of attenuation for studies of earthquake source, in *Earthquake Source Mechanics, Geophys. Monogr. Ser.*, vol. 37, edited by S. Das and C. H. Scholz, pp 311–318, AGU, Washington, D.C., 1986.

Anderson, J. G. and S. E. Hough, A model for the shape of the Fourier amplitude spectrum of acceleration at high frequencies, Bull. Seism. Soc. Am. 74, 1969–1994. *Bull. Seismol. Soc. Am.*, *74*, 1969-1994, 1984.

Andrews, D. J., Objective determination of source parameters and similarity of earthquakes of different size, in *Earthquake Source Mechanics, Geophys. Monogr. Ser.*, vol. 37, edited by S. Das and C. H. Scholz, pp 259–268, AGU, Washington, D.C., 1986.

Archuleta, R. J., E. Cranswick, C. Mueller, and P. Spudich, 1982. Source parameters of the 1980 Mammoth Lakes, California, earthquake sequence, *J. Geophys. Res.*, *87*, 4595–4608, 1982.

Bakun, W. H., C. G. Bufe, and R. M. Stewart, Do P- and S-wave corner frequencies measure different source parameters?, *U.S. Geol. Surv. Open File Rep.*, *80-607*, 1–10, 1980.

Boatwright, J., Seismic estimates of stress release, *J. Geophys. Res.*, *89*, 6961–6968, 1984.

Boatwright, J. and J. B. Fletcher, A general inversion scheme for source, site, and propagation characteristics using multiply recorded sets of moderate events, *Bull. Seismol. Soc. Am.*, *81*, 1754–1782, 1991.

Borcherdt, R. G., J. B. Fletcher, E. G. Jensen, L. Maxwell, J. R. Van Shaak, R. E. Warrick, E. Cranswick, J. S. Johnston, and R. McClearn, A general earthquake-observation system, *Bull. Seismol. Soc. Am.*, *75* , 1783-1825, 1985.

Brune, J. N., Tectonic stress and the seismic shear waves from earthquakes, *J. Geophys. Res.*, *75*, 4997–5009, 1970.

Dreger, D. S., Empirical Green's function study of the January 17, 1994 Northridge, California earthquake, *Geophys. Res. Lett.*, *21*, 2633–2636, 1994.

Frankel, A., High frequency spectral falloff of earthquakes, fractal dimension of complex rupture, b-value, and the scaling of stress on faults, *J. Geophys. Res.*, *96*, 6291–6302, 1991.

Frankel, A., Mechanisms of seismic attenuation in the crust - scattering and anelasticity in New York State, South Africa, and Southern California, *J. Geophys. Res.*, *96*, 6269–6289, 1991.

Frankel, A., J. Fletcher, F. Vernon, L. Haar, J. Berger, T. Hanks, and J. Brune, Rupture characteristics and tomographic source imaging of $M_l \approx 3$ earthquakes near Anza, southern California, *J. Geophys. Res.*, *91*, 12633–12650, 1986.

Guo, H., A. Lerner-Lam, S. E. Hough, and W. Menke, Empirical Green's function study of Loma Prieta aftershocks *U.S. Geol. Surv. Prof. Pap.*, in press, 1997.

Hanks, T. C., fmax, *Bull. Seismol. Soc. Am.*, *72*, 1867–1880, 1979.

Hanks, T. C. and D. Boore, Moment-magnitude relations in theory and practice *J. Geophys. Res.*, *89*, 6229–6235, 1984.

Haskell, N. A., Total energy and energy spectral density of elastic wave propagation from propagating faults. Part II, *Bull. Seismol. Soc. Am.*, *56*, 125–140, 1966.

Hauksson, E., L. M. Jones, K. Hutton, and D. Eberhart-Phillips, The 1992 Landers earthquake sequence-Seismological observations, *J. Geophys. Res.*, *98*, 19835–19858, 1993.

Hauksson, E., K. Hutton, H. Kanamori, L. Jones, J. Mori, S. Hough, and G. Roquemore, Preliminary report on the 1995 Ridgecrest earthquake sequence in eastern California, *Seismol. Res. Lett.*, *66*, 54–60, 1995.

Hough, S. E., Observational constraints on earthquake source scaling: understanding the limits in resolution, *Tectonophysics*, *261*, 83–96, 1996.

Hough, S. E., and J. G. Anderson, High-frequency spectra observed at Anza, California: Implications for Q structure, *Bull. Seismol. Soc. Am.*, *78*, 692–707, 1988.

Hough, S. E., and D. S. Dreger, Source parameters of the 4/23/92 Joshua Tree, California, earthquake and its aftershocks: Empirical Green's function analysis of TERRAscope and GEOS data, *Bull. Seismol. Soc. Am.*, *85*, 1576–1590, 1995.

Hough, S. E., and L. Seeber, Seismological constraints on source properties of the m_b = 4.0 Ardsley, New York earthquake: A characteristic rupture? *J. Geophys. Res.*, *96*, 18183–18195., 1991.

Hough, S. E., K. Jacob, and R. Busby, Ground motions from a M=3.5 earthquake near Massena, New York: Evidence for the poor resolution of corner frequency from small events, *Seismol. Res. Lett.*, *60*, 95–99, 1989.

Humphrey, J. R., and J. G. Anderson, Seismic source parameters from the Guerrero subduction zone, *Bull. Seismol. Soc. Am.*, *84*, 1754–1769, 1995..

Jones, L. E. and D. V. Helmberger, Seismicity and stress drop in the eastern Transverse ranges, southern California, *Geophys. Res. Lett.*, *23*, 233–236, 1996.

Joyner, W. B., R. E. Warrick, and A. A. Oliver, Analysis of seismograms from a downhole array in sediments near San Francisco Bay, *Bull. Seismol. Soc. Am.*, *66*, 937–958, 1976..

Keilis-Borok, V.I., 1959. On the estimation of the displacement of an earthquake source and of source dimension, *Ann. Geofis.*, *12*, 205-214, 1959.

Kennett, B. L. N., and N. J. Kerry, Seismic waves in a stratified half space, *Geophys. J. R. Astron. Soc.*, *57*, 557–583, 1979.

Madariaga, R., Dynamics of an expanding circular fault, *Bull. Seismol. Soc. Am.*, *66*, 639–666, 1976.

Madariaga, R., The dynamic field of Haskell's rectangular dislocation fault model, *Bull Seismol. Soc. Am.*, *68*, 869–887, 1978.

Mori, J. and S. Hartzell, Source inversion of the 1988 Upland earthquake: Determination of a fault plane for a small event, *Bull. Seismol. Soc. Am.*, *80*, 507–518, 1990.

Mueller, C.S., Source pulse enhancement by deconvolution of an empirical Green's function, *Geophys. Res. Lett.*, *12*, 33–36, 1985.

Thatcher, W. and T. C. Hanks, Source parameters of southern California earthquakes, *J. Geophys. Res.*, *78*, 8547–8574, 1973.

Walter,W. R., J.N. Brune, and K. Priestley, Observations of high frequency P-wave earthquake and explosion spectra compared with ω^{-3}, ω^{-2}, and Sharpe source models, *J. Geophys. Res.*, *93*, 6318–6324, 1988.

Wessel, P., and W.H.F. Smith, Free software helps map and display data, *Eos Trans. AGU*, *72*, 441–446, 1991.

Wyss, M. and J. N. Brune, Regional variations of source properties in Southern California estimated from the ratio of short- to long-period amplitudes, *Bull. Seismol. Soc. Am.*, *61*, 1153–1167, 1971.

S. E. Hough, 525 South Wilson Avenue, Pasadena, CA 91106 (e-mail: hough@gps.caltech.edu)

(Received March 18, 1996; revised November 5, 1996; accepted November 8, 1996.)